



Article

A Novel Missense Mutation at EDA2R Gene Identified in a Case Study Associated with Hypohidrotic Ectodermal Dysplasia

Wan Yang^{1,†}, Siyu Jin^{1,†}, Jie Jiang¹, Wei Ji^{1,2,*} and Qing He^{1,*}

¹ State Key Laboratory of Oral & Maxillofacial Reconstruction and Regeneration, Key Laboratory of Oral Biomedicine Ministry of Education, Hubei Key Laboratory of Stomatology, School & Hospital of Stomatology, Wuhan University, Wuhan 430000, China

² Department of Implantology, School & Hospital of Stomatology, Wuhan University, Wuhan 430000, China

* Correspondence: wei.ji@whu.edu.cn (W.J.); qing.he@whu.edu.cn (Q.H.);

Tel.: +86-131-0061-5376 (W.J.); +86-183-2719-2492 (Q.H.)

† These authors contributed equally as first authors.

‡ These authors share equal senior authorships.

How To Cite: Yang, W.; Jin, S.; Jiang, J.; et al. A Novel Missense Mutation at EDA2R Gene Identified in a Case Study Associated with Hypohidrotic Ectodermal Dysplasia. *Regenerative Medicine and Dentistry* 2025, 2(1), 2. <https://doi.org/10.53941/rmd.2025.100002>.

Received: 3 January 2025

Revised: 11 February 2025

Accepted: 25 February 2025

Published: 11 March 2025

Abstract: Hypohidrotic Ectodermal Dysplasia (HED) is a rare genetic disorder characterized by hypodontia, hypohidrosis, and hypotrichosis. The study aims to identify a novel mutation in the *EDA2R* gene in a 20-year-old female with HED and investigate its impact on the NF- κ B signaling pathway. Whole genome sequencing confirmed the mutation, and bioinformatic tools predicted it to be pathogenic by destabilizing the EDA2R structure and weakening its interaction with EDA-A2. Molecular dynamics simulation and binding free energy calculations further revealed reduced hydrogen bond formation in the mutant EDA2R/EDA-A2 complex, while molecular docking and AlphaFold analyses indicated decreased binding to TRAF3 and TRAF6. In vitro experiments demonstrated that cells expressing the mutant EDA2R had significantly reduced proliferation and NF- κ B activity, along with impaired nuclear translocation of NF- κ B p65. However, Western blot analysis showed that the JNK signaling pathway remained unaffected. This study identifies a novel missense mutation in *EDA2R* and introduces a new pathogenic mechanism of HED, emphasizing the crucial role of EDA2R in regulating NF- κ B signaling.

Keywords: hypohidrotic ectodermal dysplasia; ectodysplasin A2 receptor; mutation; NF- κ B

1. Introduction

Hypohidrotic Ectodermal Dysplasia (HED) is a rare genetic disorder which affects 1 in 5000–100,000 newborns [1]. It primarily affects the development of ectodermal structures, including the skin, hair, teeth, and sweat glands. Individuals with HED typically present with hypohidrosis, hypotrichosis, and hypodontia. These features arise due to mutations in several key genes crucial for the development and maintenance of ectodermal tissues, including genes encoding Ectodysplasin A (*EDA*), Ectodysplasin A Receptor (*EDAR*), and *EDAR*-associated death domain (*EDARADD*) [2–5].

The *EDA* gene family is central to the pathogenesis of HED. Mutations in the *EDA* gene lead to X-linked hypohidrotic ectodermal dysplasia, the most common form of the disorder [5,6]. The *EDA* gene encoding protein has eight isoforms resulting from alternative splicing [6]. However, only EDA-A1 (a 391-amino-acid protein) and EDA-A2 (a 389-amino-acid protein) possess a receptor-binding domain [7]. Previous studies suggest a slight



difference in crystal structures between these two isoforms, with EDA-A1 other than EDA-A2 containing Glu 308 and Val 309 in the receptor-binding region [8,9].

The different structures of receptor-binding region between EDA-A1 and EDA-A2 potentially lead to different molecular functions. EDA-A1 mainly interacts with EDAR and EDARADD, thus activating Nuclear factor- κ B (NF- κ B) signaling pathways, which regulate normal development of hair follicles, teeth, and sweat glands [10]. On the other hand, EDA2R activates the NF- κ B and JNK pathways in an EDA-A2-dependent fashion, TRAF3 and -6, IKK1/IKKalpha, IKK2/IKKbeta, and NEMO/IKKgamma are involved in EDA2R-induced NF- κ B activation, EDA2R-induced JNK activation seems to be mediated via a pathway dependent on TRAF3, TRAF6, and ASK1 [11,12]. In an early epidemiological study involving 9000 people from 8 isolated villages in a secluded region of Sardinia (Ogliastra), *EDA2R* was found to be associated with androgenetic alopecia [13].

Up to date, studies indicate that *EDA2R* is associated with androgenetic alopecia. It is also involved in muscle pathophysiology, playing a role in muscle atrophy, aging, and insulin resistance [13–15], the pathogenicity of *EDA2R* mutations leading to HED are less studied. The first documented case of an *EDA2R* mutation was observed in a 13-year-old male patient showing mild HED symptoms with a frameshift mutation (c.252delG) in *EDA2R* [16]. However, the precise role of *EDA2R* in regulating ectodermal development and homeostasis is not well understood [11].

Herein, we report a novel missense gene mutation (rs193191639, p.Thr78Asn) in the *EDA2R* found in a 20-year-old female diagnosed with HED. We performed pathogenicity predictions, protein structure modeling molecular dynamics simulations, and in vitro biological validations. Our data demonstrate that this mutation alters the protein structure, destabilizes the interaction between EDA-A2 and EDA2R, and inhibits NF- κ B signaling pathway by disrupting p65 internalization. Taken together, our study highlights the importance of understanding the genetic basis and molecular mechanisms underlying HED and related disorders, which is crucial for advancing diagnostic accuracy and developing targeted therapies. Advances in genetic research continue to enhance our knowledge of these conditions, offering hope for more effective treatments and better management strategies for HED patients.

2. Materials and Methods

2.1. Case Presentation

The proband, a 20 year-old female sought treatment at the Department of Implantology of the School and Hospital of Stomatology at Wuhan University due to the oligodontia. The principles outlined in the Declaration of Helsinki were adhered to throughout the study. The patient reported that no systematic disease. Notably, her families did not display any similar abnormalities.

2.2. Clinical and Biochemical Examinations

Basic information, medical history, and allergy history were obtained from the proband. The routine extra-oral and intra-oral examinations focusing on the proband's skin, oral mucosa, and dentition were conducted, including periodontal assessments, tooth mobility evaluations, and pulp vitality tests, which were referenced from the EAO Certificate in Implant-based Therapy Standardised Documentation for Implant Treatment. Cone beam computed tomography (CBCT) was performed for treatment planning. Blood samples were obtained from the proband, her sister and her father for routine serum biochemical tests. The Informed consents were obtained from the patient/patient's sister and father in accordance with the regulations of the Ethical Committee of School and Hospital of Stomatology at Wuhan University, as well as the 1964 Helsinki Declaration and its subsequent amendments.

2.3. Whole Genome Sequencing and Mutation Analysis

Whole-genome sequencing was performed by BGI (Shenzhen, China) using peripheral blood samples from the proband and family members. Genomic DNA was extracted with the TIANamp Blood DNA Kit (Tiangen Biotech, Beijing, China) according to the manufacturer's protocol. Sequencing was conducted on the DNBSEQ platform using combinatorial probe-anchor synthesis (cPAS), achieving an average depth of 33.87X for the proband, with 98.87% genome coverage.

Variants (SNPs, InDels) were detected using GATK4's HaplotypeCaller, and variant annotation was done via SnpEff. Structural variants (SV) and copy number variants (CNV) were identified using BreakDancer, CNVnator, and further annotated using Ensemble-VEP. Mutect2 was used for somatic variant detection. FACETS

and Manta were applied for CNV and SV detection, respectively. Final annotated variants underwent downstream analysis.

Our analysis focused on HED-related genes (*EDA*, *EDAR*, *EDARADD*, *EDA2R*, *EDA-A2*, *TRAF*, *NEMO*, *WNT10A*). Variants were filtered based on MAF <1% from the 1000 Genomes Project and NHLBI-ESP6500 cohorts, and pathogenicity was assessed using tools like SIFT, PolyPhen2, and Condel.

EDA2R(ENSG00000131080) variants were validated via PCR and Sanger sequencing using specific primers (F: ATGGATTGCCAAGAAAATGAG, R: TTAAGGGCTGGGAACCTCAA), and sequences were analyzed with Chromas for segregation within the family.

2.4. Bioinformatics Analysis

To predict the conservation of the *EDA2R* mutation site, we downloaded the protein sequences of *EDA2R* from different species using the UniProt database. Multiple sequence alignment was performed using MEGA software (version 7.0.26) to assess the conservation of the mutation site across various species [17]. The frequency of the identified mutation was determined by referencing data from the NCBI SNP database, specifically from the entry rs193191639 (<https://www.ncbi.nlm.nih.gov/snp/rs193191639>) (accessed on 6 October 2024). To predict the pathogenicity of the identified mutation, we utilized several in silico tools, including SIFT4G, PolyPhen2, MutationTaster, PROVEAN, M-CAP, MVP and REVEL [18–26].

2.5. Computational Modeling and Molecular Dynamics Simulations of Protein Structures

The amino acid sequences of the *EDA2R* and *EDA* isoforms (Q9HAV5-2 and Q92838-3) were obtained from Uniport (<https://www.uniprot.org>) (accessed on 6 October 2024). The threonine at 78th site of *EDA2R* (Q9HAV5-2) was mutated to asparagine. Alphafold2 was used to predict the initial conformations, and Pymol (v2.5.5) was employed to extract subsets with high sequence identity in functional domains, namely amino acids 1–123 of *EDA2R* and 249–389 of *EDA* [27]. Binding of TRAF3 and TRAF6 to *EDA2R* was predicted by Alphafold3 [28,29].

Molecular dynamics (MD) simulations were conducted using Amber22 [30]. Implicit solvent systems relaxation of wt(wild-type)-*EDA2R*, mut(mutant)-*EDA2R*, and wt-*EDA* was performed with Generalized Born (GB) method [31,32]. The FF19SB force field (Tian et al. 2020) was loaded with PBradii set to mbondi3. The proteins underwent 10,000 steps of both the steepest descent and conjugate gradient algorithms [33], followed by heating to 300 K in 20 ps, a 200 ps relaxation, and a final 100 ns relaxation at 300 K. The CPPTRAJ module [34] was utilized to evaluate MD trajectory and RMSD. The wt-*EDA2R* and *EDA* were docked using the ZDOCK Server [35] and the top structure was further analyzed. The docked wt-*EDA2R/EDA* complex underwent point mutation with Pymol to obtain the mut-*EDA2R/EDA* complex. MD simulations used the FF19SB force field in a 4-point OPC water box [36] with 150 mM NaCl. Energy minimization involved 20,000 cycles with 100 kcal/mol*Ang⁻² restraint. The system was heated to 300 K in 1ns under constant volume and relaxed at a constant pressure for 1ns. The restraint was reduced to 10 kcal/mol*Ang⁻² for another 1 ns NPT MD. Then, three more 1ns NPT MD simulations were performed with backbone restraints of 10, 1 and 0.1 kcal/mol*Ang⁻². Finally, the system was relaxed for 100 ns without restraint.

The MM-GBSA method [37] was used to calculate the binding free energy for two complexes. The GB solvation radii was set to mbondi2 and a total of 10 ns production was run with coordinates recorded every 10 ps. The last 500 frames were analyzed with MMPBSA.py included in AmberTools22 [3].

2.6. In Vitro Experiment

2.6.1. Cell Culture and Cell Transfection

Human embryonic kidney 293T cells (HEK293T) were cultured in high glucose DMEM medium containing 10% fetal bovine serum and 1% penicillin-streptomycin at 37 °C under 5% CO₂.

The human *EDA2R* gene (wild-type *EDA2R* or mutant *EDA2R* with c.233 C>T) was cloned into the pcDNA3.1-EGFP vector (Fenghui Biotechnology, Changsha, China) to achieve *EDA2R* overexpression. The pcDNA3.1-EGFP empty vector served as a negative control (NC). Plasmid transfection was performed using Lipofectamine 2000 (Invitrogen Corporation, Carlsbad, CA, USA) according to the manufacturer's instructions.

2.6.2. Cell Proliferation Assay

Cell proliferation was evaluated using the Cell Counting Kit-8 (CCK-8, 40203ES92, Yeasen, Shanghai, China). Briefly, 1000 transfected cells (wild-type *EDA2R*, mutant *EDA2R*, or empty pcDNA3.1-EGFP vector) were seeded into each well of a 96-well plate. After 24 h of transfection, 100 ng/mL of recombinant human EDA-A2 protein (Catalog #: 922-ED, R&D Systems) was added to the culture medium. Twelve hours later, the CCK-8 working solution was added to each well, and the plate was incubated at 37 °C with 5% CO₂ for 90 min. Absorbance at 450 nm was then measured using a microplate reader, providing a quantitative assessment of cell viability and proliferation.

2.6.3. Luciferase Reporter Assay

HEK293T cells were seeded and co-transfected with the pNF-κB-luc reporter plasmid and the pRL-TK internal control plasmid, along with one of the following: (1) wild-type *EDA2R* plasmid, (2) mutant *EDA2R* plasmid, or (3) empty pcDNA3.1-EGFP vector (EV).

After 24 h of transfection, 100 ng/mL of recombinant human EDA-A2 protein was added to each treatment group. Following a further 12-h incubation, firefly and Renilla luciferase activities were measured using the Dual-Luciferase® Reporter Assay System (Promega, Madison, WI, USA). Firefly luciferase activity was normalized to Renilla luciferase activity to account for variations in transfection efficiency.

2.6.4. RNA Extraction and Quantitative Real-Time PCR (qRT-PCR)

293T cells were treated using the same grouping, transfection, and stimulation methods as those used in the cell proliferation assay. Total RNA was then extracted using the E.Z.N.A. Total RNA Kit (Omega Bio-Tek, GA, USA) according to the manufacturer's instructions. After measuring RNA concentration, the RNA was reverse-transcribed into cDNA following the supplier's protocol. Quantitative real-time PCR (qRT-PCR) was performed using qPCR SYBR Green Master Mix (Hieff, China), and relative gene expression was calculated using the $2^{-\Delta\Delta Ct}$ method. The primers used were as follows:

EDA2R: Forward 5'-ACCTGTGCTGTCATCAATCGTGTC-3', Reverse 5'-CCTCCAATGCGTGCTTTTCGGTAG-3'.

NF-κB: Forward 5'-ATGTGGAGATCATTGAGCAGC-3', Reverse 5'-CCTGGTCCTGTGTAGCCATT-3'

GAPDH: Forward 5'-GCAAAGTGGAGATTGTTGCCAT-3', Reverse 5'-CCTTGACTGTGCCGTTGAATTT-3'.

2.6.5. Immunofluorescence

Using the same experimental protocol as before, 293T cells were transfected and stimulated. For immunofluorescence, 293T cells were fixed and permeabilized, then incubated with a primary antibody against NF-κB p65 (Abcam, Shanghai, China), followed by goat anti-rabbit IgG/RBITC secondary antibody (Solarbio, Beijing, China). Slides were mounted with anti-fade medium containing DAPI (Solarbio, Beijing, China) and imaged using a confocal microscope (FV500, Olympus, Tokyo, Japan). The immunofluorescence procedure was based on a previously published protocol [38]. Each IF assay was performed in triplicate, with at least three random fields selected per sample. NF-κB p65 fluorescence intensity was quantified using ImageJ (Version 1.8.0–172, <https://imagej.nih.gov/ij/>) (accessed on 6 October 2024).

2.6.6. Western Blot Analysis

Using the same experimental protocol as before, 293T cells were transfected and stimulated. For western blot analysis, Cells were lysed on ice in a lysis buffer (Merck Millipore) containing a proteinase inhibitor (MedChemExpress, HY-K0010, Monmouth Junction, NJ, USA) and processed by centrifugation at 13,000 rpm for 10 min at 4 °C. Protein concentrations were measured using a BCA Protein Assay Kit (Thermo Fisher Scientific, Waltham, MA, USA) according to the manufacturer's instructions. For each sample, 15 μg of denatured protein per well was loaded onto a 10% polyacrylamide gel, separated by electrophoresis, and then transferred onto nitrocellulose membranes (Millipore, Merck, Darmstadt, Germany). After blocking with 5% nonfat milk in TBST for 1 h at room temperature, membranes were incubated overnight at 4 °C with the following primary antibodies: Rabbit anti-JNK1/2/3 (1:1000; Abclonal #A4867, Wuhan, China), Rabbit anti-Phospho-SAPK/JNK (Thr183/Tyr185) (1:1000; Cell Signaling Technology #9251, Danvers, MA, USA) and Mouse anti-β-Actin (1:20,000; Proteintech #66009-1-Ig, Wuhan, China). On the next day, membranes were incubated with horseradish peroxidase-conjugated secondary antibodies diluted in 5% nonfat milk for 1 h at room temperature: Goat anti-

Rabbit IgG (Abclonal #AS014, Wuhan, China; 1:4000) and Goat anti-Mouse IgG (Abclonal #AS071, Wuhan, China; 1:4000). Signals were detected using WesternBright ECL solution (Advansta, Menlo Park, CA, USA), and densitometry analysis standardized to β -Actin was performed using Fiji software (version 2.14.0). Western blot quantifications were conducted with at least triplicates ($n = 3$) for each condition.

2.7. Statistical Analysis

Statistical analysis and data visualization were performed using GraphPad Prism version 9 software (La Jolla, CA, USA). Quantitative differences from experiments, including CCK-8, qPCR, dual-luciferase reporter assays, and p65 nuclear translocation quantification, were evaluated using a two-sample t-test. Each experiment was repeated at least three times and calculated mean \pm SEM (Standard Error of the Mean), and all tests were two-tailed. Statistical significance was indicated by asterisks: * $p < 0.05$, ** $p < 0.01$, *** $p < 0.001$, **** $p < 0.0001$.

3. Result

3.1. Clinical Manifestations

The proband is a 20-year-old female presenting with pronounced features of ectodermal dysplasia. She exhibits craniofacial abnormalities, including frontal bossing, mandibular prognathism, and maxillary hypoplasia. Her hair and eyebrows are sparse, and there is periorbital hyperpigmentation (Figure 1a). Oral examination and cone-beam computed tomography (CBCT) reveal alveolar bone hypoplasia, multiple congenitally missing teeth, with only one canine remaining in the mandible. The remaining teeth exhibit abnormal morphology, and the patient is unable to chew or achieve proper occlusion (Figure 1b–d,f). Periodontal charting, pulp vitality tests, and other relevant evaluations are included in Supplementary Table S1. Additionally, the skin on her lower limbs is dry, thin, and fragile, and shows pigmentation (Figure 1e). Based on these systemic and oral manifestations, the proband was diagnosed with hypohidrotic ectodermal dysplasia (HED).

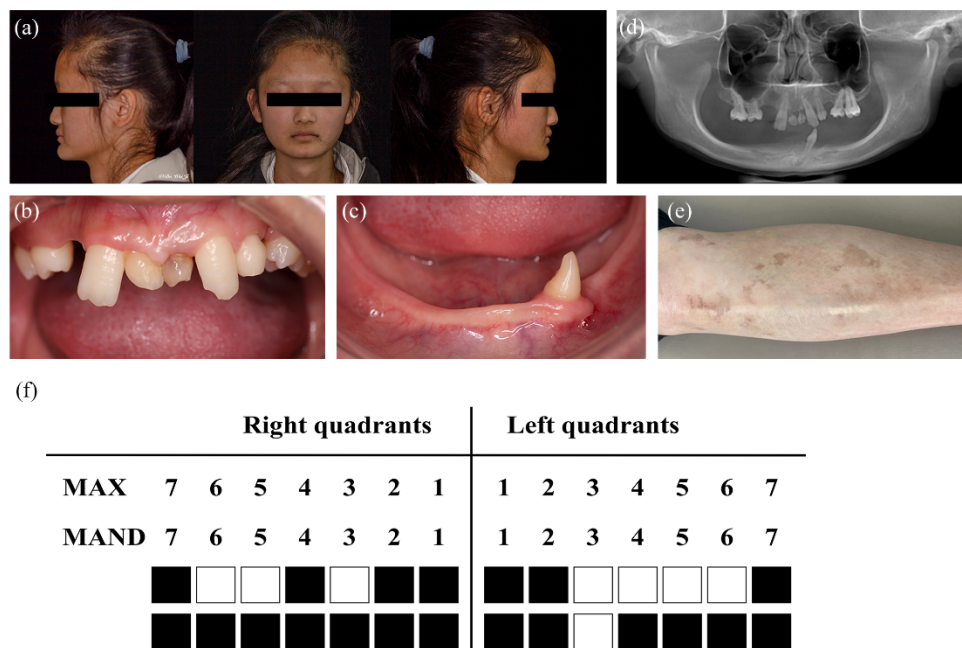


Figure 1. Patient phenotypes and clinical features. (a) Facial features of the patient diagnosed with Hypohidrotic Ectodermal Dysplasia (HED) with typical craniofacial abnormalities associated with HED. (b) Intra-oral photograph of the maxillary dentition. (c) Intra-oral photograph of the mandibular dentition. (d) Panoramic radiograph image displaying the complete dentition and jawbone structure. (e) Photograph of skin condition displaying the dry and scaly texture. (f) The diagram of permanent tooth agenesis in the proband.

3.2. Identification of EDA2R Variants

Whole genome sequencing (WGS) was performed on the patient, identifying multiple variants across the genome, and variants with a minor allele frequency (MAF) greater than 0.01 were rigorously filtered out, specifically focusing on the genes known related with HED, such as genes in NF- κ B and Wnt signaling pathways.

demonstrating the high conservation of the c.233 mutation site across various species. (c) Mutation frequency plot showcasing the rarity of the c.233 C>T mutation across different databases, including The genome Aggregation Database (gnomAD), The Exome Aggregation Consortium (ExAC), Allele Frequency Aggregator (ALFA), 1000 Genomes Project phase 3: 30X coverage whole genome sequencing (1KG_30X), 14KJPN (a Japanese reference genome panel of more than 14,000 individuals), 8.3KJPN (a Japanese reference genome panel of 8380 individuals), and the Korean Reference Genome Database (KRGDB). (d) Pathogenicity prediction heatmap illustrating the consistent categorization of the c.233 C>T mutation as likely pathogenic by multiple bioinformatics tools. Scores closer to 1 indicate a higher likelihood of pathogenicity.

3.3. Protein Conformational Analyses of EDA2R Variant

The full-length 3D structure of EDA2R was constructed using alphafold2 (Figure S1). We then utilized root mean square deviation (RMSD) to evaluate the structural stability of both wild-type (wt-EDA2R) and mutant (mut-EDA2R) forms after 100ns of Molecular Dynamics (MD) simulations. Both variants maintained an RMSD of less than 1 Å throughout the simulation (Figure S2), indicating stable structures relative to their initial conformations. However, analysis of hydrogen bonding patterns revealed notable differences between the wild-type and mutant proteins (Figure 3a). In wt-EDA2R, strong hydrogen bonds were observed between 78Thr and 51Ser (1.9 Å bond length) and between 77Ala and 50Lys (1.8 Å bond length). In contrast, in the mut-EDA2R, 78Asn did not form significant hydrogen bonds with neighboring amino acids, and the bond length between 77Ala and 50Lys increased to 2.1 Å, indicating weakened interactions. This suggests that the structural stability of amino acids around the mutation site is diminished. Further examination of the EDA2R/EDA-A2 complexes showed that the RMSD values gradually stabilized within the 100 ns relaxation phase, with no major deviations exceeding 3 Å (Figure 3b). However, the simulation results revealed a more pronounced conformational optimization of the wild-type complex compared to the mutant form (Figure 3c). By 40 ns of simulation, the wild-type complex had formed a higher number of stable intermolecular hydrogen bonds, including those between 31Cyx, 48Arg, 55Hte, 60Ser, 61Cyx, and 108Thr with the ligand, while the mutant complex had significantly fewer bonds (Figure 3d).

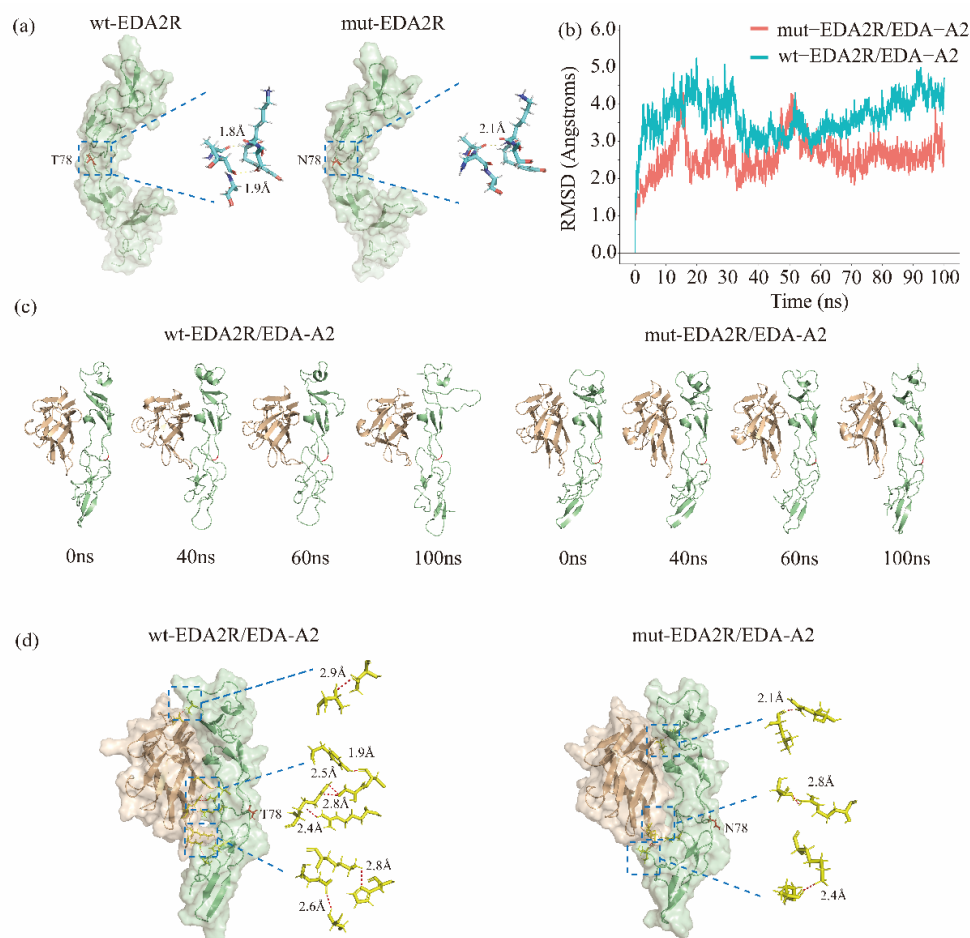


Figure 3. Molecular dynamics simulations of ectodysplasin A2 receptor (EDA2R) and its complex. (a) The structure of wt-EDA2R and mut-EDA2R after 100 ns MD simulation. Critical residues near the 78th red labelled

residue were shown as sticks, with hydrogen bonds (in angstroms) indicated by yellow dashed lines. (b) The root mean square deviation (RMSD) results for wild-type and mutant EDA2R/EDA complexes within 100 ns relaxation without any restraint. (c) The structure of wild-type and mutant EDA2R/EDA complexes after 0, 40, 60 and 100 ns MD simulation. The 78th residue was colored red. (d) The structure of wild-type and mutant EDA2R/EDA complexes after 10 ns MD simulation. Hydrogen bonding (in angstroms) between complexes was demonstrated with stick models.

Binding free energy calculations using the MM-GBSA method further supported these observations, that the wt-EDA2R/EDA-A2 complex had a significantly lower total binding free energy (-34.8028 kcal/mol) compared to the mutant complex (-23.2907 kcal/mol) (Table S4). This suggests that the wildtype EDA2R has a more energetically favorable interaction with the EDA-A2 ligand, enhancing both the hydrophobicity and stability of the complex. Conversely, mutant EDA2R has a weaker affinity for its ligand, which may lead to inhibition of subsequently signaling pathways. These findings underline the structural and functional impacts of the c.233 C>T mutation on the EDA2R protein, providing insights into its role of HED pathogenesis.

We further analyzed the predicted binding structures of TRAF3 and TRAF6 with EDA2R using AlphaFold3. The wild-type EDA2R/TRAF3 complex formed five intermolecular hydrogen bonds, compared to only four in the mutant EDA2R/TRAF3 complex. Similarly, the wild-type EDA2R/TRAF6 complex exhibited three hydrogen bonds, while the mutant EDA2R/TRAF6 complex formed only one (Figure S3). These findings suggest that the c.233 C>T mutation in EDA2R reduces its ability to establish stable interactions with TRAF3 and TRAF6, potentially impairing downstream NF- κ B signaling.

3.4. Functional Assessment of EDA2R Variant

To evaluate the functional impact of the c.233 C>T mutation, HEK-293T cells were transfected with plasmids expressing either wild-type *EDA2R*, mutant *EDA2R*, or an empty vector (EV, pcDNA3.1-EGFP). Twenty-four hours post-transfection, the cells were stimulated with 100 ng/mL of EDA-A2 and incubated for an additional 12 h. Cell proliferation was then assessed using the CCK-8 assay. Compared to the wild-type group, cells transfected with the mutant plasmid or the empty vector showed a markedly reduced proliferative capacity ($p < 0.0001$, Figure 4a), indicating that the c.233 C>T mutation significantly impairs cell proliferation.

Next, we conducted a dual-luciferase reporter assay to further investigate how the c.233 C>T mutation affects NF- κ B signaling. Compared with cells expressing wild-type EDA2R, those carrying the mutant EDA2R exhibited significantly reduced luciferase activity ($p = 0.0032$). Moreover, the empty vector group demonstrated markedly lower activity relative to both the wild-type and mutant groups, likely due to the absence of EDA2R expression and thus a diminished response to external ligand stimulation (Figure 4b). Taken together, these findings confirm that the c.233 C>T mutation substantially impairs NF- κ B signaling, supporting our hypothesis that this mutation compromises the receptor's ability to effectively activate this critical pathway.

In addition, we performed qPCR analysis on HEK-293T cells transfected with wild-type, mutant *EDA2R*, or the empty vector (EV). As expected, *EDA2R* expression in the EV group was negligible, with relative expression levels approaching zero compared to the wild-type and mutant groups (Figure S4). Next, we normalized *NF- κ B* expression levels to those of *EDA2R*, enabling a direct comparison of the *NF- κ B/EDA2R* ratio between cells expressing wild-type and mutant *EDA2R*. The results revealed a significant reduction in the *NF- κ B/EDA2R* ratio in the mutant *EDA2R* group compared to the wild-type group (Figure 4c). These findings further confirm that the c.233 C>T mutation impairs EDA2R-mediated NF- κ B signaling, disrupting the receptor's normal regulatory function.

When the NF- κ B pathway is activated, the p65 subunit translocates into the cell nucleus [37]. To examine whether the c.233 C>T mutation affects this nuclear translocation, we performed immunofluorescence microscopy. In cells expressing wild-type EDA2R, p65 fluorescence was predominantly localized in the nucleus following EDA-A2 stimulation, indicating successful nuclear translocation. In contrast, cells expressing the mutant EDA2R displayed markedly reduced nuclear accumulation of p65, with no visible nuclear aggregates indicative of robust translocation (Figure 4d). Quantitative analysis of p65 fluorescence intensity further supported this observation, showing a significant decrease in nuclear p65 levels in the mutant group compared to the wild-type group ($p = 0.0061$, Figure 4e). These findings are consistent with our qPCR and dual-luciferase reporter assay results, reinforcing the conclusion that the c.233 C>T mutation disrupts the receptor's ability to facilitate proper NF- κ B activation and p65 nuclear localization.

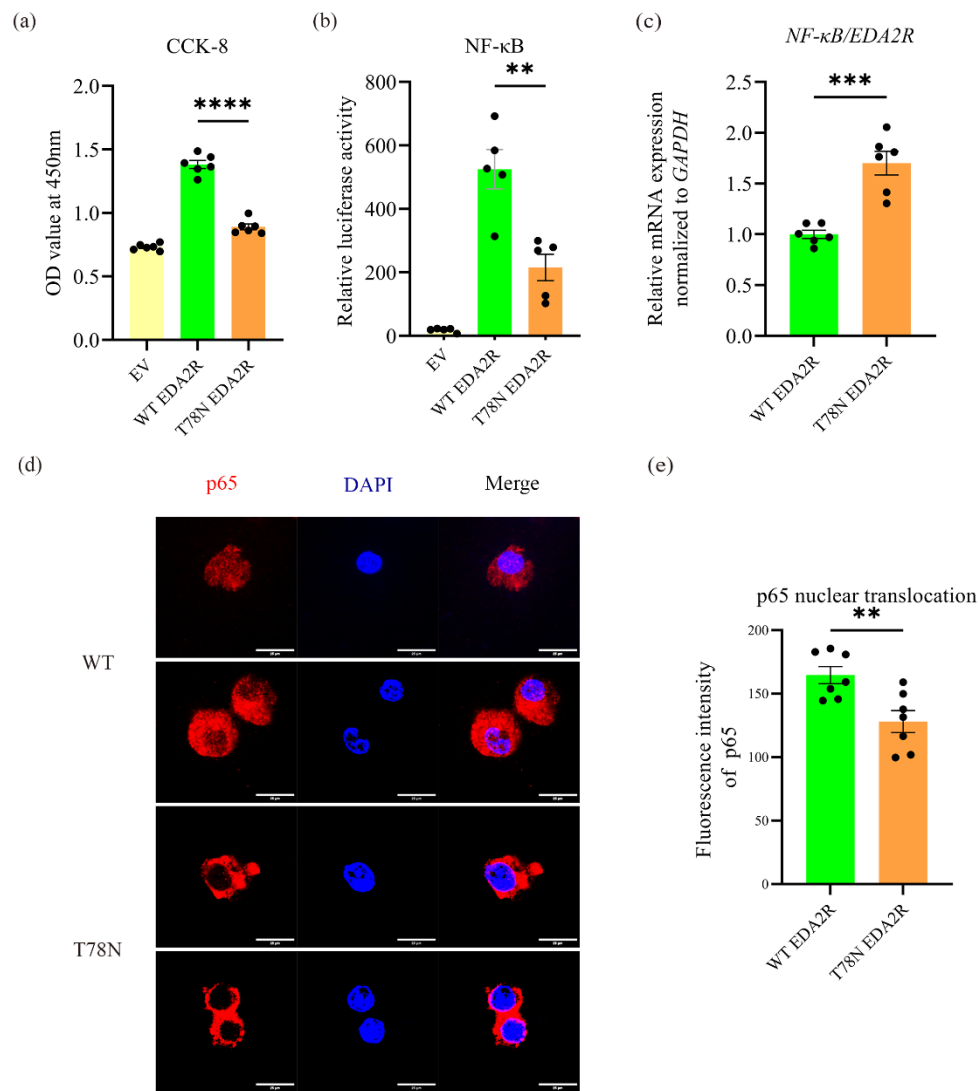


Figure 4. Analysis of cellular and molecular effects of wild-type and mutant ectodysplasin A2 receptor (EDA2R) plasmids in HEK-293T cells. (a) CCK-8 assay showing cell proliferation of HEK-293T cells transfected with WT, Mutant (T78N), or EV plasmids after EDA-A2 stimulation (n = 6). **** $p < 0.0001$ Mut vs. WT. (b) Dual-luciferase reporter assay demonstrating reduced NF- κ B transcriptional activity in cells HEK-293T cells transfected with WT, Mutant or EV *EDA2R* plasmids (n = 5). *** $p < 0.001$ Mut vs. WT. (c) qPCR analysis of *NF- κ B* expression normalized to *EDA2R* in HEK-293T cells transfected with WT, Mutant or EV *EDA2R* plasmids (n = 6). ** $p < 0.01$ Mut vs. WT. (d) Immunofluorescence staining of NF- κ B p65 (red) in HEK-293T cells transfected with WT or Mutant *EDA2R* plasmids following EDA-A2 stimulation. Nuclei are counterstained with DAPI (blue). Representative images from two of eight independent experiments are shown. (e) Quantification of nuclear p65 fluorescence intensity in cells transfected with WT, T78N, or EV *EDA2R* plasmids (n = 8). ** $p < 0.01$ vs. WT. Data are presented as mean \pm SEM.

According to published reports, EDA2R and EDA-A2 are also involved in regulating the JNK signaling pathway [12]. Therefore, in this study, we used Western blot to further examine the activation and expression of the JNK pathway in different groups of cells following EDA-A2 stimulation. The data showed that there were no significant differences in JNK pathway activation (p-JNK/JNK) among the groups (Figure S5). Taken together, these findings demonstrate that the c.233 C>T mutation in the *EDA2R* gene significantly disrupts normal cellular functions by impairing proliferation, altering NF- κ B signaling, and affecting the expression and localization of key regulatory proteins.

4. Discussion

Ectodermal dysplasias (ED) are a heterogeneous group of disorders that are characterized by abnormal development of ectodermal structures like hair, teeth, nails, and sweat glands. Among these, hypohidrotic ectodermal dysplasia (HED) is the most prevalent form, primarily affecting hair growth, sweat gland function, and dental morphology. HED is typically associated with mutations in key components of the EDA signaling pathway and WNT pathway [38–40]. The ectodysplasin/NF- κ B signaling axis is critical for the proper development of ectodermal tissues, and disruptions in this pathway have been shown to underlie many of the clinical features seen in HED patients. A report has revealed that EDA1, EDAR, and EDARADD, are responsible for 90% of cases of HED [4]. Additionally, mutations in EDAR account for 25% of non-EDA-related HED cases [41].

In this study, we identified a novel missense mutation, c.233 C>T in the *EDA2R* gene from a female patient presenting with typical HED phenotypes, including craniofacial abnormalities, sparse hair, hypodontia, and dry, fragile skin. While mutations in *EDA*, *EDAR*, and *EDARADD* are commonly associated with HED, mutations in *EDA2R* are exceedingly rare, with only a handful of cases previously described [16]. Previous reports of *EDA2R* mutations, such as the c.252delG frameshift mutation, have demonstrated that disruptions in *EDA2R*'s structure can lead to non-functional proteins, resulting in mild to moderate HED phenotypes [16]. The c.233 C>T missense mutation described here further highlights the critical role of *EDA2R* in maintaining the structural integrity and signaling capacity of ectodermal tissues.

Our molecular dynamics simulations and structural analysis revealed that the c.233 C>T mutation significantly impacts the structure and function of the *EDA2R* protein. Although both the wild-type and mutant forms of *EDA2R* maintained overall structural stability during the simulation, the missense mutation caused significant alterations in hydrogen bonding patterns, particularly at the mutation site (Thr78Asn). Meanwhile, the reduced intermolecular hydrogen bonds are all located between the TNF homology domain (THD) of EDAA2 and *EDA2R*. Previous research has proven that mutations in the THD impair the binding of EDAA2 to its receptor [42]. Therefore, these disruptions likely impair the protein's ability to interact effectively with its ligand, EDAA2. This conclusion is supported by the reduced number and strength of intermolecular hydrogen bonds in the mutant *EDA2R*/EDA-A2 complex compared to the wild-type complex, as well as the higher binding free energy observed in the mutant complex. These findings suggest that the c.233 C>T mutation reduces the binding affinity and structural stability of the *EDA2R*/EDA-A2 interaction.

The altered structural dynamics of the mutant *EDA2R* is highly likely to compromise its ability to activate downstream NF- κ B signaling pathway, an essential pathway regulating the development of ectodermal tissues including hair follicles, teeth, and sweat glands, which are hallmarks of HED [43]. NF- κ B activation is mediated through two main pathways: the canonical and non-canonical pathways [44]. *EDA2R* has been shown to activate the canonical pathway by interacting with TRAF6, leading to the nuclear translocation of NF- κ B dimers, including p50/RelA, which bind to the promoters of NF- κ B-responsive genes. Additionally, *EDA2R* can activate the non-canonical pathway through TRAF3, leading to the processing of p100 to p52 and the nuclear translocation of the p52/RelB complex [10]. Protein interaction modeling showed that the wild-type *EDA2R* formed more hydrogen bonds with TRAF3 and TRAF6, suggesting a tighter, stronger interaction with potentially greater stability. Hydrogen bonds contribute to the formation of stable molecular interactions, and the wild-type complex may be more likely to maintain activity within the cell. In contrast, after the mutation, the stability of the binding between *EDA2R* and TRAF3/TRAF6 decreased, which could lead to reduced signal transduction efficiency and affect the activation and expression of downstream genes.

Our in vitro experiments confirmed that c.233 C>T mutation in *EDA2R* gene led to an impaired NF- κ B signaling. Cells transfected with the mutant *EDA2R* plasmid exhibited significantly reduced proliferation compared to those transfected with the wild-type plasmid, suggesting that the mutation impairs normal cellular growth. This finding aligns with previous studies showing that NF- κ B signaling plays a key role in promoting cell survival and proliferation [45].

The dual-luciferase reporter assay and qPCR analyses revealed that NF- κ B signaling was markedly diminished in cells expressing the mutant *EDA2R*, indicating that the c.233 C>T mutation disrupts the receptor's ability to activate this critical signaling pathway. The reduction in p65 nuclear translocation observed in immunofluorescence assays further supports the hypothesis that the c.233 C>T mutation interferes with the receptor's ability to effectively activate NF- κ B signaling. Given that NF- κ B regulates a wide array of genes involved in cell survival, differentiation, and immune responses, the impairment of this pathway could explain many of the clinical manifestations observed in the patient, including defective tooth development, sparse hair, and fragile skin.

EDA2R is involved in both NF- κ B and JNK signaling pathways. It activates NF- κ B in an EDA-A2-dependent manner through TRAF3, TRAF6, IKKs, and NEMO, while JNK activation seems to be mediated by TRAF3, TRAF6, and ASK1 [12]. To determine whether this mutation affects the JNK signaling pathway, we examined the phosphorylation levels of JNK before and after the mutation via Western blot. The results showed that this mutation did not significantly impact the activation of the JNK pathway.

5. Conclusion

In summary, our study identified a novel missense mutation in *EDA2R* gene, which mutation disrupts the structural and functional integrity of the EDA2R protein, and impairs the receptor's ability to interact with its ligand, EDA-A2, leading to diminished NF- κ B signaling and downstream effects on cell proliferation and ectodermal development. Our data provide new insights into the molecular mechanisms underlying HED and highlight the importance of EDA2R in maintaining ectodermal tissue integrity. Furthermore, our data also highlights the potential therapeutic implications of understanding the molecular basis of EDA2R-related HED. For instance, small molecules or biologics that enhance NF- κ B activation downstream of the receptor could potentially mitigate some of the clinical symptoms associated with HED. Additionally, early genetic diagnosis could play a crucial role in predicting disease progression and guiding treatment strategies. Future studies should focus on expanding our understanding of EDA2R mutations in larger patient cohorts and exploring potential therapeutic strategies to restore normal signaling in affected individuals. Moreover, our results provide a theoretical basis for the development of targeted therapies for HED patients and will help guide further functional studies in this field.

Supplementary Materials

The additional data and information can be downloaded at: <https://www.sciltp.com/journals/rmd/2025/1/691/s1>. Figure S1: Conformation of EDA2R predicted by alphafold2; Figure S2: The RMSD results for wild-type and mutant EDA2R within 100 ns relaxation; Figure S3: The predicted structure of EDA2R/TRAF complexes; Figure S4: Quantitative PCR (qPCR) Analysis of *EDA2R* mRNA Expression in HEK-293T Cells Transfected with Wild-Type *EDA2R*, Mutant *EDA2R*, or Empty Vector (EV) (n = 6). Data are presented as mean \pm SEM; Figure S5: Western blot analysis was performed to measure the expression of the JNK signaling pathway (n = 3). Data are presented as mean \pm SEM. Table S1: Periodontal charting, pulp vitality tests, and other relevant evaluations; Table S2: Results of pathogenicity prediction; Table S3: Selection and exclusion of potentially pathogenic genes; Table S4: Binding free energy results by MM-GBSA (kcal/mol).

Author Contributions

W.Y.: Writing—original draft, methodology, investigation, data curation; S.J.: Writing—original draft, Software, methodology, data curation; J.J.: Data curation; Q.H.: Writing—review & editing, funding acquisition, conceptualization, supervision; W.J.: Writing—review & editing, funding acquisition, conceptualization, supervision. All authors have read and agreed to the published version of the manuscript.

Funding

This work received financial supports from National Natural Science Foundation of China (82072483 to He Q), the Natural Science Foundation of Hubei Province (ZRMS2020000955), the Key Research and Development Program of Hubei Province (2022BCA052), and the International Team of Implantology (ITI) Research Foundation (1721–2022).

Institutional Review Board Statement

Conducted the study in accordance with the Declaration of Helsinki.

Informed Consent Statement

Informed consent was obtained from all subjects involved in the study.

Data Availability Statement

The datasets used and/or analyzed during the current study are available from the corresponding author on reasonable request.

Acknowledgments

The authors are grateful to the and their family members for their participation in this study. We also appreciate the clinical support from Bin Huang, and Jiali Zhang from the Department of Implantology, School and Hospital of Stomatology, Wuhan University.

Conflicts of Interest

The authors declare no competing interests.

References

1. Wright, J.T.; Grange, D.K.; Fete, M. Hypohidrotic Ectodermal Dysplasia. In *GeneReviews®*; Adam, M.P., Feldman, J., Mirzaa, G.M., et al., Eds.; University of Washington: Seattle, WA, USA, 2003. Available online: <https://www.ncbi.nlm.nih.gov/books/NBK1112/> (accessed on 6 October 2024).
2. Lefebvre, S.; Mikkola, M.L. Ectodysplasin Research—Where to Next? *Semin. Immunol.* **2014**, *26*, 220–228. <https://doi.org/10.1016/j.smim.2014.05.002>.
3. Yu, K.; Huang, C.; Wan, F.; et al. Structural Insights into Pathogenic Mechanism of Hypohidrotic Ectodermal Dysplasia Caused by Ectodysplasin a Variants. *Nat. Commun.* **2023**, *14*, 767. <https://doi.org/10.1038/s41467-023-36367-6>.
4. Cluzeau, C.; Hadj-Rabia, S.; Jambou, M.; et al. Only Four Genes (EDA1, EDAR, EDARADD, and WNT10A) Account for 90% of Hypohidrotic/Anhidrotic Ectodermal Dysplasia Cases. *Hum. Mutat.* **2011**, *32*, 70–72. <https://doi.org/10.1002/humu.21384>.
5. Aftab, H.; Escudero, I.A.; Sahhar, F. X-Linked Hypohidrotic Ectodermal Dysplasia (XLHED): A Case Report and Overview of the Diagnosis and Multidisciplinary Modality Treatments. *Cureus* **2023**, *15*, e40383. <https://doi.org/10.7759/cureus.40383>.
6. Fan, H.; Ye, X.; Shi, L.; et al. Mutations in the EDA Gene Are Responsible for X-linked Hypohidrotic Ectodermal Dysplasia and Hypodontia in Chinese Kindreds. *Eur. J. Oral Sci.* **2008**, *116*, 412–417. <https://doi.org/10.1111/j.1600-0722.2008.00555.x>.
7. Liu, X.; Zhao, Y.; Zhu, J. A Novel Mutation in the Collagen Domain of EDA Results in Hypohidrotic Ectodermal Dysplasia by Impacting the Receptor-binding Capability. *Mol. Gen. Gen. Med.* **2023**, *11*, e2119. <https://doi.org/10.1002/mgg3.2119>.
8. Yan, M.; Wang, L.-C.; Hymowitz, S.G.; et al. Two-Amino Acid Molecular Switch in an Epithelial Morphogen That Regulates Binding to Two Distinct Receptors. *Science* **2000**, *290*, 523–527. <https://doi.org/10.1126/science.290.5491.523>.
9. Hymowitz, S.G.; Compaan, D.M.; Yan, M.; et al. The Crystal Structures of EDA-A1 and EDA-A2. *Structure* **2003**, *11*, 1513–1520. <https://doi.org/10.1016/j.str.2003.11.009>.
10. Gao, Y.; Jiang, X.; Wei, Z.; et al. The EDA/EDAR/NF-κB Pathway in Non-Syndromic Tooth Agenesis: A Genetic Perspective. *Front. Genet.* **2023**, *14*, 1168538. <https://doi.org/10.3389/fgene.2023.1168538>.
11. Verhelst, K.; Gardam, S.; Borghi, A.; et al. XEDAR Activates the Non-Canonical NF-κB Pathway. *Biochem. Biophys. Res. Commun.* **2015**, *465*, 275–280. <https://doi.org/10.1016/j.bbrc.2015.08.019>.
12. Sinha, S.K.; Zachariah, S.; Quiñones, H.I.; et al. Role of TRAF3 and -6 in the Activation of the NF-κB and JNK Pathways by X-Linked Ectodermal Dysplasia Receptor. *J. Biol. Chem.* **2002**, *277*, 44953–44961. <https://doi.org/10.1074/jbc.M207923200>.
13. Prodi, D.A.; Pirastu, N.; Maninchedda, G.; et al. EDA2R Is Associated with Androgenetic Alopecia. *J. Investig. Dermatol.* **2008**, *128*, 2268–2270. <https://doi.org/10.1038/jid.2008.60>.
14. Özen, S.D.; Kir, S. Ectodysplasin A2 Receptor Signaling in Skeletal Muscle Pathophysiology. *Trends Mol. Med.* **2024**, *30*, 471–483. <https://doi.org/10.1016/j.molmed.2024.02.002>.
15. Lolli, F.; Pallotti, F.; Rossi, A.; et al. Androgenetic Alopecia: A Review. *Endocrine* **2017**, *57*, 9–17. <https://doi.org/10.1007/s12020-017-1280-y>.
16. Wisniewski, S.A.; Trzeciak, W.H. A New Mutation Resulting in the Truncation of the TRAF6-Interacting Domain of XEDAR: A Possible Novel Cause of Hypohidrotic Ectodermal Dysplasia: Figure 1. *J. Med. Genet.* **2012**, *49*, 499–501. <https://doi.org/10.1136/jmedgenet-2012-100877>.
17. Zeng, B.; Lu, H.; Xiao, X.; et al. Novel EDA Mutation in X-linked Hypohidrotic Ectodermal Dysplasia and Genotype–Phenotype Correlation. *Oral Dis.* **2015**, *21*, 994–1000. <https://doi.org/10.1111/odi.12376>.
18. Raimondi, D.; Tanyalcin, I.; Ferté, J.; et al. DEOGEN2: Prediction and Interactive Visualization of Single Amino Acid Variant Deleteriousness in Human Proteins. *Nucleic Acids Res.* **2017**, *45*, W201–W206. <https://doi.org/10.1093/nar/gkx390>.
19. Jagadeesh, K.A.; Wenger, A.M.; Berger, M.J.; et al. M-CAP Eliminates a Majority of Variants of Uncertain Significance in Clinical Exomes at High Sensitivity. *Nat. Genet.* **2016**, *48*, 1581–1586. <https://doi.org/10.1038/ng.3703>.
20. Ioannidis, N.M.; Rothstein, J.H.; Pejaver, V.; et al. REVEL: An Ensemble Method for Predicting the Pathogenicity of Rare Missense Variants. *Am. J. Hum. Genet.* **2016**, *99*, 877–885. <https://doi.org/10.1016/j.ajhg.2016.08.016>.

21. Vaser, R.; Adusumalli, S.; Leng, S.N.; et al. SIFT Missense Predictions for Genomes. *Nat. Protoc.* **2016**, *11*, 1–9. <https://doi.org/10.1038/nprot.2015.123>.
22. Quang, D.; Chen, Y.; Xie, X. DANN: A Deep Learning Approach for Annotating the Pathogenicity of Genetic Variants. *Bioinformatics* **2015**, *31*, 761–763. <https://doi.org/10.1093/bioinformatics/btu703>.
23. Choi, Y.; Sims, G.E.; Murphy, S.; et al. Predicting the Functional Effect of Amino Acid Substitutions and Indels. *PLoS ONE* **2012**, *7*, e46688. <https://doi.org/10.1371/journal.pone.0046688>.
24. Adzhubei, I.A.; Schmidt, S.; Peshkin, L.; et al. A Method and Server for Predicting Damaging Missense Mutations. *Nat. Methods* **2010**, *7*, 248–249. <https://doi.org/10.1038/nmeth0410-248>.
25. Schwarz, J.M.; Cooper, D.N.; Schuelke, M.; et al. MutationTaster2: Mutation Prediction for the Deep-Sequencing Age. *Nat. Methods* **2014**, *11*, 361–362. <https://doi.org/10.1038/nmeth.2890>.
26. Qi, H.; Zhang, H.; Zhao, Y.; et al. MVP Predicts the Pathogenicity of Missense Variants by Deep Learning. *Nat. Commun.* **2021**, *12*, 510. <https://doi.org/10.1038/s41467-020-20847-0>.
27. Mirdita, M.; Schütze, K.; Moriwaki, Y.; et al. ColabFold: Making Protein Folding Accessible to All. *Nat. Methods* **2022**, *19*, 679–682. <https://doi.org/10.1038/s41592-022-01488-1>.
28. Jumper, J.; Evans, R.; Pritzel, A.; et al. Highly Accurate Protein Structure Prediction with AlphaFold. *Nature* **2021**, *596*, 583–589. <https://doi.org/10.1038/s41586-021-03819-2>.
29. Varadi, M.; Bertoni, D.; Magana, P.; et al. AlphaFold Protein Structure Database in 2024: Providing Structure Coverage for over 214 Million Protein Sequences. *Nucleic Acids Res.* **2024**, *52*, D368–D375. <https://doi.org/10.1093/nar/gkad1011>.
30. Case, D.A.; Aktulga, H.M.; Belfon, K.; et al. AmberTools. *J. Chem. Inf. Model.* **2023**, *63*, 6183–6191. <https://doi.org/10.1021/acs.jcim.3c01153>.
31. Nguyen, H.; Maier, J.; Huang, H.; et al. Folding Simulations for Proteins with Diverse Topologies Are Accessible in Days with a Physics-Based Force Field and Implicit Solvent. *J. Am. Chem. Soc.* **2014**, *136*, 13959–13962. <https://doi.org/10.1021/ja5032776>.
32. Onufriev, A.V.; Case, D.A. Generalized Born Implicit Solvent Models for Biomolecules. *Annu. Rev. Biophys.* **2019**, *48*, 275–296. <https://doi.org/10.1146/annurev-biophys-052118-115325>.
33. Zhao, Z.; Zhang, T.; Li, T.; et al. A Novel EDAR Variant Identified in Non-Syndromic Tooth Agenesis: Insights from Molecular Dynamics. *Arch. Oral Biol.* **2023**, *146*, 105600. <https://doi.org/10.1016/j.archoralbio.2022.105600>.
34. Roe, D.R.; Cheatham, T.E. PTRAJ and CPPTRAJ: Software for Processing and Analysis of Molecular Dynamics Trajectory Data. *J. Chem. Theory Comput.* **2013**, *9*, 3084–3095. <https://doi.org/10.1021/ct400341p>.
35. Pierce, B.G.; Wiehe, K.; Hwang, H.; et al. ZDOCK Server: Interactive Docking Prediction of Protein–Protein Complexes and Symmetric Multimers. *Bioinformatics* **2014**, *30*, 1771–1773. <https://doi.org/10.1093/bioinformatics/btu097>.
36. Izadi, S.; Anandakrishnan, R.; Onufriev, A.V. Building Water Models: A Different Approach. *J. Phys. Chem. Lett.* **2014**, *5*, 3863–3871. <https://doi.org/10.1021/jz501780a>.
37. Miller, B.R.; McGee, T.D.; Swails, J.M.; et al. MMPBSA.Py: An Efficient Program for End-State Free Energy Calculations. *J. Chem. Theory Comput.* **2012**, *8*, 3314–3321. <https://doi.org/10.1021/ct300418h>.
38. Dufour, W.; Alawbathani, S.; Jourdain, A.-S.; et al. Monoallelic and Biallelic Variants in LEF1 Are Associated with a New Syndrome Combining Ectodermal Dysplasia and Limb Malformations Caused by Altered WNT Signaling. *Genet. Med.* **2022**, *24*, 1708–1721. <https://doi.org/10.1016/j.gim.2022.04.022>.
39. Yu, M.; Fan, Z.; Wong, S.W.; et al. *Lrp6* Dynamic Expression in Tooth Development and Mutations in Oligodontia. *J. Dent. Res.* **2021**, *100*, 415–422. <https://doi.org/10.1177/0022034520970459>.
40. Ahmed, H.A.; El-Kamah, G.Y.; Rabie, E.; et al. Gene Mutations of the Three Ectodysplasin Pathway Key Players (EDA, EDAR, and EDARADD) Account for More than 60% of Egyptian Ectodermal Dysplasia: A Report of Seven Novel Mutations. *Genes* **2021**, *12*, 1389. <https://doi.org/10.3390/genes12091389>.
41. Chassaing, N.; Bourthoumieu, S.; Cossee, M.; et al. Mutations in EDAR Account for One-Quarter of Non-ED1-Related Hypohidrotic Ectodermal Dysplasia. *Hum. Mutat.* **2006**, *27*, 255–259. <https://doi.org/10.1002/humu.20295>.
42. Schneider, P.; Street, S.L.; Gaide, O.; et al. Mutations Leading to X-Linked Hypohidrotic Ectodermal Dysplasia Affect Three Major Functional Domains in the Tumor Necrosis Factor Family Member Ectodysplasin-A *. *J. Biol. Chem.* **2001**, *276*, 18819–18827. <https://doi.org/10.1074/jbc.M101280200>.
43. Petersheim, D.; Massaad, M.J.; Lee, S.; et al. Mechanisms of Genotype–Phenotype Correlation in Autosomal Dominant Anhidrotic Ectodermal Dysplasia with Immune Deficiency. *J. Allergy Clin. Immunol.* **2018**, *141*, 1060–1073.e3. <https://doi.org/10.1016/j.jaci.2017.05.030>.
44. Hoesel, B.; Schmid, J.A. The Complexity of NF- κ B Signaling in Inflammation and Cancer. *Mol. Cancer* **2013**, *12*, 86. <https://doi.org/10.1186/1476-4598-12-86>.
45. Hayden, M.S.; Ghosh, S. Regulation of NF- κ B by TNF Family Cytokines. *Semin. Immunol.* **2014**, *26*, 253–266. <https://doi.org/10.1016/j.smim.2014.05.004>.